IEEE Access
Multidisciplinary ⋮ Rapid Review ⋮ Open Access Journal

Received 17 April 2024, accepted 3 May 2024, date of publication 8 May 2024, date of current version 15 May 2024.

Digital Object Identifier 10.1109/ACCESS.2024.3397953

RESEARCH ARTICLE

MIMO Radar Mainlobe Gain Control Design for Co-Existence With Wireless Communication Systems

OMAR ALDAYEL, (Member, IEEE)
Department of Electrical Engineering, King Saud University (KSU), Riyadh 11421, Saudi Arabia
Prince Sultan Advanced Technologies Research Institute (PSATRI), Riyadh 13244, Saudi Arabia
e-mail: omaldayel@ksu.edu.sa

ABSTRACT We tackle the issue of designing a transmit beampattern for multiple-input multiple-output (MIMO) radar while considering its coexistence with wireless communication systems. Our goal is to design a beampattern that can steer the mainlobe and regulate its gain level toward the desired direction. The significant challenge lies in concurrently enforcing the gain constraint along with the constant modulus constraint on the radar waveform. In our work, we propose a novel approach that entails solving a series of constrained quadratic programs to achieve constant modulus at convergence. Additionally, we demonstrate that each problem in the sequence admits a closed-form solution, ensuring analytical tractability. We assess the effectiveness of our proposed Mainlobe and Interference Control (MAIC) algorithm against state-of-the-art MIMO beampattern design techniques, illustrating that MAIC attains the desired gain level while mitigating interference energy in undesired areas.

INDEX TERMS Beampattern design, co-existence, constant modulus, electronic steering, main lobe energy constraint, MIMO radar, successive algorithm.

I. INTRODUCTION

With the advent of next generation millimeter wave wireless systems and the newly emerging high-resolution radars, the radio spectrum has become extremely crowded. One issue that has been discussed lately is the risk of the spectrum overlapping between 5G wireless systems emissions and radar systems. Recently, the Federal Communications Commission (FCC) assigned a C-Band radio spectrum (3.7-3.98 GHz) to operate 5G wireless communication which is very close to radar altimeters spectrum used by commercial aircrafts [1], [2]. For that reason, the Federal Aviation Administration (FAA) exchanged information with the 5G operators and radar altimeter manufacturers to ensure aviation safety [3]. Ultimately, more work is needed at the practical and theoretical fronts to tackle such issues.

In the literature, the co-existence of radar and telecommunication systems has been studied [4], [5], [6], [7], [8], [9], [10], [11], [12], [13], [14], [15]. A priori knowledge about the locations of radio frequency users is required to avoid the interference with each other. Specifically, the MIMO radar/wireless telecommunication systems should focus the radiation beam at the expected target/receiver while maintaining a low interference energy level at other geographic areas assigned to other licensed wireless systems. These requirements could be achieved by constrained mathematical optimization of the transmit beampattren [16], [17].

The optimization of radar waveform to match a desired spectrum shape has been a topic of much recent interest [18], [19], [20], [21], [22], [23], [24], [25], [26], [27], [28], [29], [30], [31], [32], [33], [34], [35], [36], [37]. In these methods, the goal of the optimization problem is to minimize the total amount of energy at the unlicensed spectrum but not sharing any frequency bands. However, since the beampattern is not considered in these studies, it is not able to control the radiation beam in spatial directions. Some other studies tackle the spatial domain by beampattern design at the receive side [26], [32], [33] or at the transmit side [19], [38]. The joint spatial and spectral design was studied in [39], and [40]. Nevertheless, the recent literature ignore or simplify some of

The associate editor coordinating the review of this manuscript and approving it for publication was Zaharias D. Zaharis.

important aspects in the optimization process which could cause unpractical or often unusable beampattern/waveform design.

A. MOTIVATION AND CHALLENGES

In practical scenarios, the design of the transmit beampattern is more problematic for several reasons. Foremost among these is the necessity to adhere to the constant modulus constraint (CMC) governing the radar transmit waveform, ensuring a consistent envelope for the transmission signal. Constant modulus requirement is very crucial for high power transmission. To achieve the maximum transmission gain, the signal is transmitted near or at the saturation region (the non-linear region) of the high-power amplifiers. As a result, the output signal will be a distorted version of the output unless it is a constant modulus signal where the envelope of the transmit signal is constant. However, this requirement may not be relevant for the receiver side. Since beamforming is concerned with the received signal, the CMC can be relaxed. In general, the problem formulation for beamforming does not have any constraints, which makes it simpler. The significance of maintaining this constant modulus waveform has been extensively documented and scrutinized for its impact on performance, as detailed in [41], [42], and [43].

More important, electronic beam steering constitutes a critical aspect of array antennas, enable microwave and millimeter wave radar systems to detect and track targets [44]. Ensuring spatial compatibility between contemporary radars and telecommunication systems introduces another important requirement: the need for electronic gain control and steering constraint.

Some past efforts have aimed to directly enforce the constant modulus constraint, leading to improved performance. However, these approaches typically involve semi-definite relaxation (SDR) with randomization [45], [46]. This entails solving a semi-definite programming (SDP) problem to determine a waveform distribution, followed by generating a large number of random waveforms based on this distribution. Subsequently, an exhaustive search is conducted to identify the waveform that best satisfies the constraint. Despite the success of SDR in addressing constant modulus constrained problems, two main challenges persist: first, extending these techniques to incorporate gain and steering control, which involve quadratic inequalities, is not straightforward; second, the computational burden associated with these methods remains high.

The design of beampatterns under the constant modulus constraint, excluding gain control and steering constraints, has been explored in several studies [15], [19], [20], [21], [30], [31], [47]. In these studies, approaches have been developed to approximate the constant modulus using the peak-to-average power ratio (PAPR) waveform constraint [27], [30]. Although the constant modulus constraint is not directly incorporated into the optimization process, the resulting solution is adjusted to the nearest constant modulus solution post-optimization. Similarly, as mentioned before there is active interest in radar-comm co-existence where the transmit waveform is optimized but without the constant modulus constraint [4], [6], [7], [8], [12], [13], [14]. To the best of our knowledge, no work considers the constant modulus and mainlobe energy constraints jointly.

In some recent development, neural networks have been utilized in beampattern design/beamforming optimizations and have shown promising results [48], [49], [50], [51], [52]. Nevertheless, their current application relies on unconstrained problems or problems having at most one constraint.

A noteworthy approach to the joint design and operation of shared spectrum access for radar and communications (SSPARC) [13]. Their work focuses on optimizing transmit waveforms at both radar and communication nodes to maximize signal power through the forward channels (main beam) of radar and communication systems, while simultaneously minimizing interference in the co-channels between radar and communications. This optimization can also extend to achieving low probability of intercept capability in specific angular keep-out zones where [13] (as well as other studies that design beam patterns for co-existence) lies in the inclusion of the hard gain control constraint as well as CMC.

B. OUR CONTRIBUTIONS

Our principal aim is to develop an algorithmic approach for steerable main lobe with a *minimum gain constraint* MIMO beampattern design. Closeness to an ideal beampattern that limits radar energy in the direction of wireless communication receivers while maintaining a large directive gain at the targets.

Specifically, this paper makes the following contributions:

- **An algorithmic solution beampattern design under both the 'main lobe gain' constraint and the constant modulus constraint.** To address the aforementioned challenges, we've devised a novel algorithm for MIMO beampattern design. This approach tackles the complex non-convex constraint of main lobe and breaking it down into a series of convex inequality constrains. This sequential approach will convergence to constant modulus.
- **Feasibility of algorithm.** Provided that the initial non-convex challenge of beampattern design is feasible, i.e. the constant modulus and gain constraints intersect effectively, we formally establish that every quadratic program (QP) formulated within the MAIC sequence mentioned earlier is also guaranteed to be feasible.
- **Convergence of the MAIC algorithm.** We demonstrate that the sequence of cost functions representing the overall interference energy is non-increasing, (indicating improvement) with each problem solved in the sequence, ultimately converging.
- **Experimental validation.** Experimental validation is conducted in two main scenarios: 1) mainlobe design with a single interference sector, where the MAIC algorithm exhibits notable power suppression in desired region despite the gain constraint, and 2) mainlobe

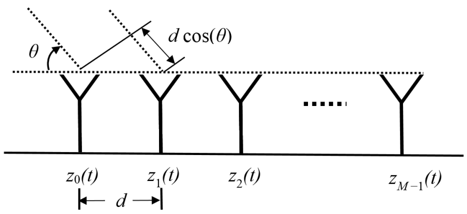

FIGURE 1. Configuration of ULA antenna.

steering problem, wherein the proposed MAIC achieves the desired gain at the target/receiver direction while reducing the energy at the unlicensed areas.

The rest of the paper is organized as follows. Section II provides brief background on the structure of the radar antenna array and the corresponding design criterion and shows the problem formulation details. Section III develops the proposed MAIC algorithm for beampattern design and reports derivations of its analytical properties. Section IV evaluates the proposed MAIC method against state-of-the-art alternatives. Concluding remarks with directions for future work are presented in Section V.

C. NOTATION

We denote vectors and matrices by boldface letters, e.g. $\mathbf{a}$ (lowercase) and $\mathbf{A}$ (uppercase), respectively. The l-th element of $\mathbf{a}$ is denoted by $\mathbf{a}_l$ and the element located in the m-th row and l-th column of the matrix $\mathbf{A}$ is denoted by $\mathbf{A}(m,l)$. We denote by $\|\mathbf{a}\|_2$ the l_2 norm of the vector $\mathbf{a}$. The Hermitian, conjugate and transpose operators are denoted by $(.)^H$, $(.)^*$ and $(.)^T$, respectively. For a complex number a, we denote $\mathfrak{Re}(a)$ and $\mathfrak{Im}(a)$ to the real and imaginary part a, respectively; also we denote $|a|$ and $\arg a$ to the amplitude and phase of a, respectively. We use $j = \sqrt{-1}$ as the imaginary unit number. Finally, we use $\otimes$ to denote the Kronecker product.

II. SYSTEM MODEL

Consider a MIMO radar having a uniform linear array (ULA) of M antennas and a spacing distance of d as shown in Fig. 1. The signal transmitted from the m-th element is denoted by $z_m(t)$. Let $z_m(t) = x_m y(t) e^{j2\pi f_c t}$ where $y(t)$ is the baseband signal and f_c is the carrier frequency. Here, $y(t)$ is assumed to be a narrowband signal (i.e. $B \ll f_c$ where B is the bandwidth in Hz) and $x_m \in \mathbb{C}$ is the *complex* wight of the m-th element.

The beampattern at the angle θ for a $\frac{\lambda}{2}$ ULA in the far-field can be given by

$$P(\theta) = |\mathbf{a}^H(\theta)\mathbf{x}|^2 \tag{1}$$

where

$$\mathbf{a}(\theta) = [1 \quad e^{j\pi \sin\theta} \ \ldots \ e^{j(M-1)\pi \sin\theta}]^T \tag{2}$$

and

$$\mathbf{x} = [x_0 \quad x_1 \quad \ldots \quad x_{M-1}]^T \tag{3}$$

Defining the electrical angle as $\xi = \pi \sin\theta$, the ULA beamforming gain is expressed as:

$$G(\xi) = \left|\sum_{m=0}^{M-1} x_m e^{-jm\xi}\right| \tag{4}$$

The total energy transmitted in the spatial range $\Xi^k = [\xi_1^k, \xi_2^k]$ can be expressed as

$$E_k = \frac{1}{2\pi}\int_{\xi_1^k}^{\xi_2^k} G^2(\xi)d\xi = \mathbf{x}^H\mathbf{G}_k\mathbf{x} \tag{5}$$

where $\mathbf{G}_k$ is an $M \times M$ matrix defined as

$$\mathbf{G}_k(i,j) = \begin{cases} \dfrac{\xi_2^k - \xi_1^k}{2\pi}, & \text{if } i = j \\ \dfrac{e^{j\xi_2^k(i-j)} - e^{j\xi_1^k(i-j)}}{2j\pi(i-j)}, & \text{otherwise} \end{cases} \tag{6}$$

Therefore, using Parseval theorem, the total energy E_T of CM vector $\mathbf{x}$ is given by:

$$E_T = \frac{1}{2\pi}\int_{-\pi}^{\pi} G^2(\xi)d\xi = \mathbf{x}^H\mathbf{x} \tag{7}$$

On the other hand, the mainbeam total energy should be larger than some threshold value E_0. The total mainlobe energy in the spatial range $\Delta = [\delta_1, \delta_2]$ can be expressed as:

$$E_{ML} = \frac{1}{2\pi}\int_{\delta_1}^{\delta_2} G^2(\xi)d\xi = \mathbf{x}^H\mathbf{M}\mathbf{x} \geq E_0 \tag{8}$$

where $\mathbf{M}$ is defined as

$$\mathbf{M}(i,j) = \begin{cases} \dfrac{\delta_2 - \delta_1}{2\pi}, & \text{if } i = j \\ \dfrac{e^{j\delta_2(i-j)} - e^{j\delta_1(i-j)}}{j2\pi(i-j)}, & \text{otherwise} \end{cases} \tag{9}$$

We would like to conceder the following the minimization problem with mainbeam control:

$$\begin{cases} \min\limits_{\mathbf{x}} f(\mathbf{x}) = \sum_{k=1}^{K} c_k\mathbf{x}^H\mathbf{G}_k\mathbf{x} - c_0\mathbf{x}^H\mathbf{M}\mathbf{x} \\ \text{s.t.:} \qquad \mathbf{x}^H\mathbf{M}\mathbf{x} \geq E_0 \\ \qquad\quad |\mathbf{x}| = \mathbf{1}, \\ \qquad\quad \mathbf{A}_0^H\mathbf{x} = \mathbf{0} \end{cases} \tag{10}$$

III. PROPOSED SOLUTION

Problem (10) is a non-convex NP-hard problem due to the CMC ($|\mathbf{x}| = \mathbf{1}$) and main lobe constraint ($\mathbf{x}^H\mathbf{M}\mathbf{x} \geq E_0$). While the CMC has been well tackled in the literature [53], [54], and [55] by iterative algorithms, the main lobe constraint has not been considered yet. There are two main challenges with the main lobe constraint: Firstly, it is a non-convex constraint that needs an accurate convex relaxation. Secondly, the feasible set of the CMC is already very tight, therefore, adding another constraint will make it even more *tighter*. Therefore, any solution to this problem must ensure the feasibility of the joint CMC and main lobe constraint all together.

In the following, we will tackle the non-convexity of the problem of the main lobe constraint. Problem (10) covert the quadratic in quality constraint to a linear one, we have the following ob servation:

Lemma 1: Let $\mathbf{M} \in \mathbb{C}^{M\times M}$ be a positive-definite Hermitian matrix having the following eigenvalues: $\lambda_1 > \lambda_2 > \ldots > \lambda_M$ corresponding to the eigenvectors $\mathbf{v}_1, \mathbf{v}_2, \ldots, \mathbf{v}_L$, respectively. Then:

$$\Re\mathfrak{e}\{\mathbf{v}_i^H\mathbf{x}\} \geq \sqrt{\frac{E_0}{\lambda_i}} \tag{11}$$

for any $\lambda_i \geq E_0$, implies that $\mathbf{x}^H\mathbf{M}\mathbf{x} \geq E_0$.

Proof. see Appendix subsection A.

Remark: For small spatial ranges Δ, the matrix $\mathbf{M}$ usually have one dominant eigenvalue λ_1 (i.e. $\mathbf{x}^H\mathbf{M}\mathbf{x} \geq \lambda_i\mathbf{x}\mathbf{v}_i\mathbf{v}_i^H\mathbf{x}$). This is the case in general, since the mainlobe in most applications should be as narrow as possible. Therefore, we will use the dominant eigenvalue $\lambda_i = \lambda_1$ in our optimization problem.

Using Lemma 1, problem (10) becomes:

$$\begin{cases} \min\limits_{\mathbf{x}} f(\mathbf{x}) = \sum_{k=1}^{K} c_k\mathbf{x}^H\mathbf{G}_k\mathbf{x} - c_0\mathbf{x}^H\mathbf{M}\mathbf{x} \\ \text{s.t.:} \quad \Re\mathfrak{e}\{\mathbf{v}_1^H\mathbf{x}\} \geq \sqrt{\frac{E_0}{\lambda_1}} \\ \quad |\mathbf{x}| = \mathbf{1}, \\ \quad \mathbf{A}_0^H\mathbf{x} = \mathbf{0} \end{cases} \tag{12}$$

Moreover, problem (12) can be converted to the following function with *real* (as opposed to complex) variables:

$$\begin{cases} \min\limits_{\mathbf{s}} \quad \mathbf{s}^T(\mathbf{R}+\beta\mathbf{I})\mathbf{s} \\ \text{s.t.:} \quad \mathbf{s}^T\mathbf{E}_l\mathbf{s} = 1, \quad l = 1, 2, \ldots, M \\ \quad \mathbf{u}^T\mathbf{s} \geq \sqrt{\frac{E_0}{\lambda_1}} \\ \quad \mathbf{B}_0^T\mathbf{s} = \mathbf{0} \end{cases} \tag{13}$$

where β is an arbitrary positive number,

$$\mathbf{s} = [\Re\mathfrak{e}\{\mathbf{x}\}^T \Im\mathfrak{m}\{\mathbf{x}\}^T]^T,$$

$$\mathbf{R} = \begin{bmatrix} \Re\mathfrak{e}\{\mathbf{P}\} & -\Im\mathfrak{m}\{\mathbf{P}\} \\ \Im\mathfrak{m}\{\mathbf{P}\} & \Re\mathfrak{e}\{\mathbf{P}\} \end{bmatrix},$$

$$\mathbf{P} = \sum_{k=1}^{K} c_k\mathbf{G}_k - c_0\mathbf{M},$$

$$\mathbf{B}_0 = \begin{bmatrix} \Re\mathfrak{e}\{\mathbf{A}_0\} & -\Im\mathfrak{m}\{\mathbf{A}_0\} \\ \Im\mathfrak{m}\{\mathbf{A}_0\} & \Re\mathfrak{e}\{\mathbf{A}_0\} \end{bmatrix},$$

and

$$\mathbf{u} = [\Re\mathfrak{e}\{\mathbf{v}_1^H\} \; \Im\mathfrak{m}\{\mathbf{v}_1^H\}]^T.$$

A. ALGORITHM STEPS

For the CMC in the optimization problem (13), we will use the same relaxation method used in BIC algorithm [39], [40]. It involves solving a sequence of convex problems. First, let us consider the following sequence of constrained QPs where the n-th QP is given by

$$(CP)^{(n)} \begin{cases} \min\limits_{\mathbf{s}} \quad \mathbf{s}^T(\mathbf{R}+\lambda\mathbf{I})\mathbf{s} \\ \text{s.t.:} \quad \mathbf{B}_c^{(n)}\mathbf{s} = \mathbf{1} \\ \quad \mathbf{B}_0^T\mathbf{s} = \mathbf{0} \\ \quad \mathbf{u}^{(n)T}\mathbf{s} \geq \sqrt{\frac{E_0}{\lambda_1}} \end{cases} \tag{14}$$

where $\mathbf{B}_c^{(n)} = [\mathbf{b}_{c1}^{(n)}, \mathbf{b}_{c2}^{(n)}, \ldots, \mathbf{b}_{cM}^{(n)}]^T \in \mathbb{R}^{M\times 2M}$ such that the line defined by $\mathbf{b}_{cl}^{(n)T}\mathbf{s} = 1$ is a tangent to the circle $\mathbf{s}^T\mathbf{E}_l\mathbf{s} = 1$ for $l = 1, 2, \ldots, M$. Specifically, $\mathbf{b}_l$ is given by

$$\mathbf{b}_{cl}^{(n)}(i) = \begin{cases} \cos(\gamma_l^{(n)}) & \text{if } i = l \\ \sin(\gamma_l^{(n)}) & \text{if } i = l+M \\ 0 & \text{otherwise.} \end{cases} \tag{15}$$

for $l = 1, \ldots, M$ where $\gamma_l^{(n)} = 2\arg(x_l^{(n-1)}) - \gamma_l^{(n-1)}$ and $x_l^{(n)}$ is the l-th elements of $\mathbf{x}^{(n)}$ which is the complex version of the optimal solution of (14), $\mathbf{s}^{(n)}$, that is, $x_l^{(n)} = s_l^{(n)} + js_{l+M}^{(n)}$ and conversely $\mathbf{s}^{(n)} = [\Re\mathfrak{e}\{\mathbf{x}^{(n)}\}^T \Im\mathfrak{m}\{\mathbf{x}^{(n)}\}^T]^T$ and $\mathbf{u}^{(n)}$ is given by:

$$\mathbf{u}^{(n)} = \begin{bmatrix} \Re\mathfrak{e}\{\mathbf{v}_1^* e^{-j\arg(\mathbf{v}_1^H\mathbf{x}^{(n-1)})}\} \\ \Im\mathfrak{m}\{\mathbf{v}_1^* e^{-j\arg(\mathbf{v}_1^H\mathbf{x}^{(n-1)})}\} \end{bmatrix} \tag{16}$$

Without the main lobe constraint ($\mathbf{u}^{(n)T}\mathbf{s} \geq \sqrt{\frac{E_0}{\lambda_1}}$), it has been shown in [40] that sequence of the resulting problems are always feasible by the construction made in eq. (14). Note that, the vector $\mathbf{u}^{(n)}$ is changes with each iteration n. In the following we prove that the sequence problem is always feasible for the joint main lobe constraint and CMC.

Lemma 2: The feasible set of problem $CP^{(n)}$ contains the optimal solution of problem $CP^{(n-1)}$.

Proof. see Appendix subsection B.

Problem (14) is a convex quadratic minimization with linear constraints. It has been shown that the solution of this problem is:

$$\mathbf{s}^{(n)} = \bar{\mathbf{R}}^{-1}\mathbf{B}^{(n)^T}\left(\mathbf{B}^{(n)}\bar{\mathbf{R}}^{-1}\mathbf{B}^{(n)^T}\right)^{-1}\mathbf{1} \tag{17}$$

where

$$\mathbf{B}^{(n)} = \begin{bmatrix} \mathbf{B}_c^{(n)} \\ \mathbf{B}_0^{(n)} \end{bmatrix} \tag{18}$$

If $\mathbf{s}^{(n)}$ satisfies $\mathbf{u}^{(n)T}\hat{\mathbf{s}}^{(n)} - \sqrt{\frac{E_0}{\lambda_1}} \geq 0$. Otherwise,

$$\mathbf{s}^{(n)} = \mu^{(n)}\bar{\mathbf{R}}^{-1}(\mathbf{I} - \mathbf{B}^{(n)^T}\hat{\mathbf{R}}\mathbf{B}^{(n)}\bar{\mathbf{R}}^{-1})\mathbf{u}^{(n)} + \hat{\mathbf{s}}^{(n)} \tag{19}$$

where

$$\hat{\mathbf{R}} = \left(\mathbf{B}^{(n)}\bar{\mathbf{R}}^{-1}\mathbf{B}^{(n)^T}\right)^{-1} \tag{20}$$

$$\mu^{(n)} = \frac{1}{\alpha^{(n)}}\left(\mathbf{u}^{(n)T}\hat{\mathbf{s}}^{(n)} - \sqrt{\frac{E_0}{\lambda_i}}\right) \tag{21}$$

$$\alpha^{(n)} = -\begin{bmatrix} \mathbf{u}^{(n)} \\ \mathbf{0} \end{bmatrix}^T \begin{bmatrix} \bar{\mathbf{R}} & \mathbf{B}^{(n)^T} \\ \mathbf{B}^{(n)} & \mathbf{0} \end{bmatrix}^{-1} \begin{bmatrix} \mathbf{u}^{(n)} \\ \mathbf{0} \end{bmatrix} \tag{22}$$

Algorithm 1 Mainlobe and Interference Control (MAIC)

Inputs: $\mathbf{G}_k$, c_k, for $k = 0, 1, 2, .., K$, $\mathbf{M}$ and ζ (the stopping threshold).
Output: A solution $\mathbf{x}^\star$ for problem (10).
(1) Set $n = 1$ and an initial value for $\mathbf{x}^{(0)}$.
(2) Compute $\mathbf{B}_c^{(n)}$ as in (15).
(3) Compute $\hat{\mathbf{s}}^{(n)}$ via eq. (17) and $\mathbf{u}^{(n)}$ via eq. (16).
(4) Check the following:
if $\bar{\mathbf{s}}^{(n)T}\hat{\mathbf{s}}^{(n)} - \sqrt{\frac{E_0}{\lambda_i}} \geq 0$ **then**
$\mathbf{s}^{(n)} = \hat{\mathbf{s}}^{(n)}$.
else
$\mathbf{s}^{(n)} = \mu^{(n)}\bar{\mathbf{R}}^{-1}(\mathbf{I} - \mathbf{B}^{(n)^T}\hat{\mathbf{R}}\mathbf{B}^{(n)}\bar{\mathbf{R}}^{-1})\mathbf{u}^{(n)} + \hat{\mathbf{s}}^{(n)}$
where $\mu^{(n)}$ is defined in (21).
end if
(5) Construct $\mathbf{x}^{(n)}$ where $x_l^{(n)} = s_l^{(n)} + js_{l+M}^{(n)}$ for $l = 1, \ldots, M$. Check the following:
if $f(\mathbf{x}^{(n)}) - f(\mathbf{x}^{(n-1)}) < \zeta$ **then**
STOP.
else
set $n = n + 1$ GOTO step (2).
end if
Output: $\mathbf{x}^\star = \exp\{j \arg(\mathbf{x}^{(n)})\}$.

The value of the objective function of the problem (14) is monotonically decreasing in each iteration n. We have the following theorem:

Theorem 1: Define $g(\mathbf{s}) = \mathbf{s}^T(\mathbf{R} + \lambda\mathbf{I})\mathbf{s}$. Then

$$g(\mathbf{s}^{(n-1)}) \geq g(\mathbf{s}^{(n)}) \tag{23}$$

In other words, the sequence $\{g(\mathbf{s}^{(n)})\}_{n=0}^{\infty}$ is non-increasing. Moreover, the sequence $\{g(\mathbf{s}^{(n)})\}_{n=0}^{\infty}$ converges to a finite value $g^\star$.

Proof. see Appendix subsection C.

Computational Complexity: The main computational cost in the MAIC algorithm comes from solving the linear system of equation (17) in each iteration, the overall computational complexity of BIC is $\mathcal{O}(FM^{2.373}) - \mathcal{O}(FM^3)$ [56] where F is the total number of iterations.

IV. NUMERICAL RESULTS

We assess the effectiveness of the proposed MAIC by comparing it with the following established methods:

- **Phase-only variable metric method (POVMM) [19]:** POVMM achieves null forming beampattern design by optimizing the waveform phases under the constant modulus constraint, without incorporating any main lobe energy constraint.
- **Successive closed forms method (SCF) [53]:** Same as POVMM but with a better performance and a faster convergence.
- **JDO SSPARC [13]:** An approach to beamforming that aims to maximize signal power through forward channels while minimizing response at co-channels.

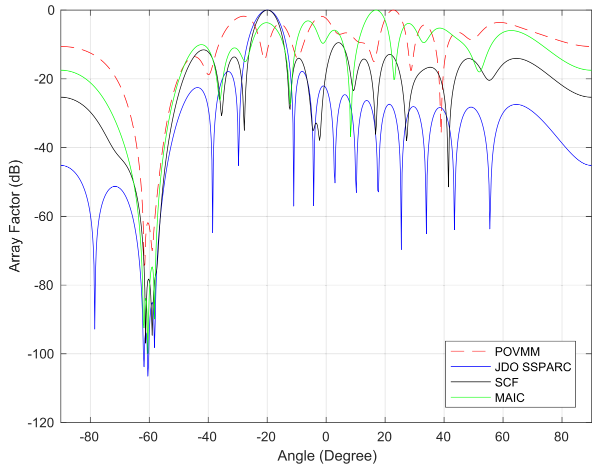

FIGURE 2. Plot of the beampattern of a single interference sector.

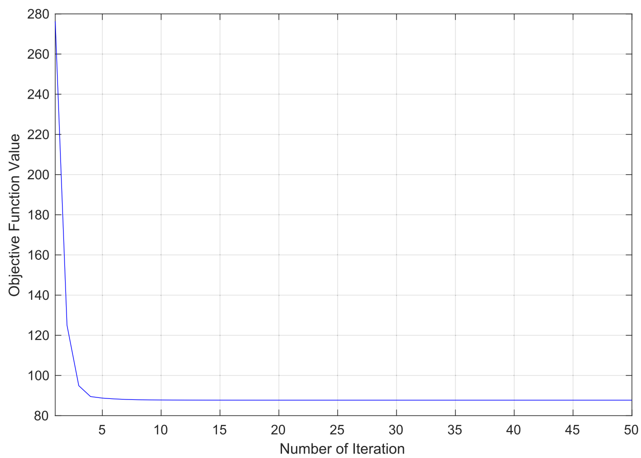

FIGURE 3. Plot of the beampattern of a single interference sector.

A. MAINLOBE DESIGN WITH A SINGLE INTERFERENCE SECTOR

We compare the proposed algorithm to state-of-the-art phase-only variable metric method (POVMM) method [19], JDO SSPARC [13] and successive closed forms method (SCF) [53]. The numerical set up is as follows: We simulate a ULA of $M = 16$ elements with half-wavelength spacing. In Algorithm 1 we set $\zeta = 10^{-5}$. Further, the interfernce spatial range is set to be $\Xi = [-62°, -58°]$ and the mainlobe energy in the spatial range $\Delta = [-18°, -22°]$.

Fig. 2 shows the results for null forming beampattern of MAIC versus POVMM, SCF and JDO SSPARC. Note that, the result of JDO SSPARC design is not constant modulus (energy constraint only), it is used here as a benchmark for the other methods. The proposed MAIC method provides an excellent interference energy suppression, better than POVMM and comparable to SCF, while maintaining the desired mainlobe at $-20°$. In Fig. 3, the value of the objective function of the MAIC algorithm decrease rapidly in each iteration until convergence at around about 12 iterations. The time response of this scenario for different antenna sizes $M = 8, 16, 32, 64$ is shown in Table 1. The computer used

TABLE 1. Time response of the MAIC algorithm.

Array size M	Time per iteration (ms)	Time until convergence (ms)
8	0.6	3.3
16	0.64	7.44
32	0.78	9.3
64	2.5	29.4

in this numerical simulation was an Apple iMAC with M1 chip and 8 GB of RAM running MATLAB version 2023b.

B. MAINLOBE DESIGN WITH TWO INTERFERENCE SECTORS

In Fig. 4, we examine the proposed algorithm for multiple interference sectors. Namely, we assume three interference sectors: $\Xi_1 = [-62°, -58°]$ and $\Xi_2 = [15°, 20°]$. MAIC method has been plotted with two different energy levels $E_0 = 1.6$ and $E_0 = 0$ (no main lobe constraint). The other numerical set up is the same as in section IV-A: a ULA of $M = 16$ elements with half-wavelength spacing, $\zeta = 10^{-5}$ and the mainlobe energy in the spatial range $\Delta = [-18°, -22°]$. For no mainbeam constraint ($E_0 = 0$), it seems that the MAIC method outperform the state-of-art methods, thanks to the new construction of the objective function to capture the total energy and not only for some specific points as in POVMM or SCF. In this case, the minimum attenuation in the sector $\Xi_2 = [15°, 20°]$ is around -61.8 dB versus -50.5 dB and -41.9 dB for SCF and POVMM, respectively. Remarkably, if the mainlobe energy increased to $E_0 = 1.6$, the minimum attenuation of MAIC method is still better than POVMM and slightly above SCF at -48 dB while maintaining a mainlobe at $-20°$.

In Fig. 5, we show the same set-up but with higher mainlobe energy values, namely, $E_0 = 4$ and $E_0 = 3.52$. Depending on the application, $E_0 = 3.52$ seems to have the best trade-off between minimum attenuation and high mainlobe energy. At $E_0 = 4$, the MAIC method could not reduce the energy at $\Xi_1 = [-62°, -58°]$ very well, however, it has the lowest side-lobe level at around -10.4 dB.

C. MAINLOBE DESIGN WITH MULTIPLE INTERFERENCE SECTORS

In Fig. 6, we examine the proposed algorithm for multiple interference sectors. Namely, we assume three interference sectors: $\Xi_1 = [-61°, -59°]$, $\Xi_2 = [10°, 30°]$ and $\Xi_3 = [50°, 70°]$. MAIC method has been plotted with two different energy levels $E_0 = 1.6$ and $E_0 = 0$ (no main lobe constraint). The other numerical set up is the same as in section IV-A: a ULA of $M = 16$ elements with half-wavelength spacing, $\zeta = 10^{-5}$ and the mainlobe energy in the spatial range $\Delta = [-18°, -22°]$. Again, for no mainbeam constraint ($E_0 = 0$), the MAIC method outperform the state-of-art methods, thanks to the new construction of the objective function to capture the total energy and not only for some specific points as in POVMM or SCF. For example, the minimum attenuation in the sector $\Xi_2 = [15°, 20°]$ is around -31.4 dB versus -23.8 dB and -23.7 dB for SCF and POVMM, respectively.

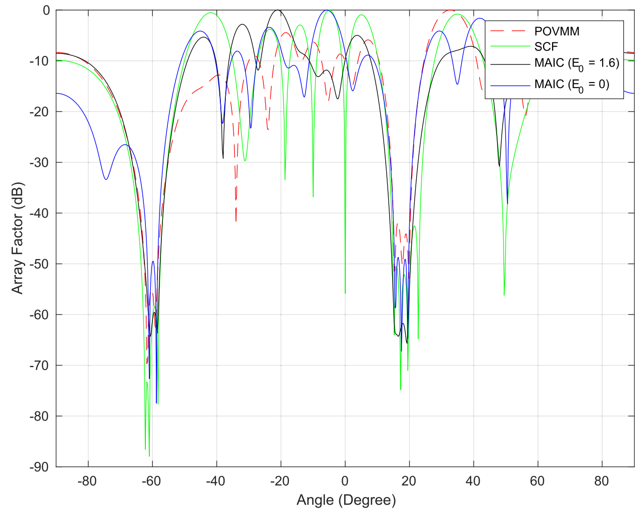

FIGURE 4. Plot of the beampattern of two interference sectors at $\Xi_1 = [-62°, -58°]$ and $\Xi_2 = [15°, 20°]$. MAIC method performance for $E_0 = 1.6$ (black line) and $E_0 = 0$ (Blue line).

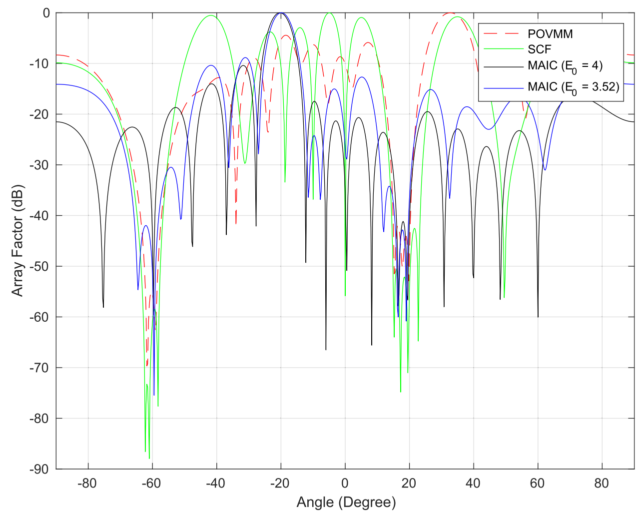

FIGURE 5. Plot of the beampattern of two interference sectors at $\Xi_1 = [-62°, -58°]$ and $\Xi_2 = [15°, 20°]$. MAIC method performance for $E_0 = 4$ (black line) and $E_0 = 3.52$ (Blue line).

Remarkably, if the mainlobe energy increased to $E_0 = 1.6$, the minimum attenuation of MAIC method is still better than POVMM as well as SCF at -28.8 dB while maintaining a mainlobe at $-20°$.

In Fig. 7, we show the same set-up but with higher mainlobe energy values, namely, $E_0 = 4$ and $E_0 = 3.52$. Depending on the application, $E_0 = 3.52$ seems to have the best trade-off between minimum attenuation and high mainlobe energy. At $E_0 = 4$ (very high mainlobe), the MAIC method could not reduce the energy at $\Xi_1 = [-62°, -58°]$ very well having the lowest side-lobe level at around -18.3 dB.

D. MAINLOBE STEERING PERFORMANCE

In Fig. 8, the mainlobe steering performance of the algorithm is shown with a couple of interference sectors. Namely,

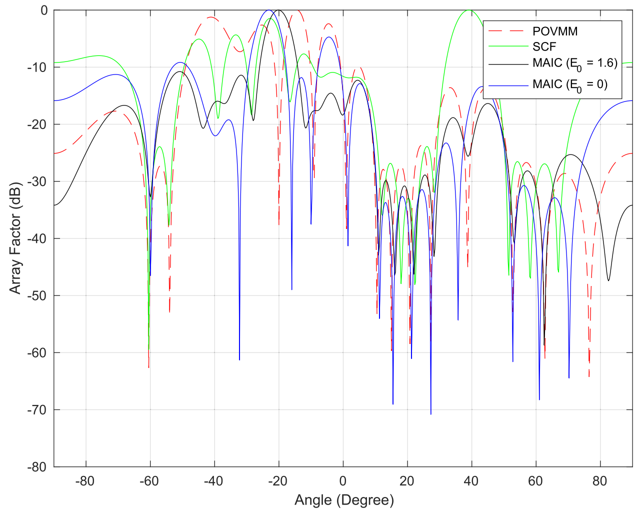

FIGURE 6. Plot of the beampattern of three interference sectors at $\Xi_1 = [-61°, -59°]$, $\Xi_2 = [10°, 30°]$ and $\Xi_3 = [50°, 70°]$. MAIC method performance for $E_0 = 1.6$ (black line) and $E_0 = 0$ (Blue line).

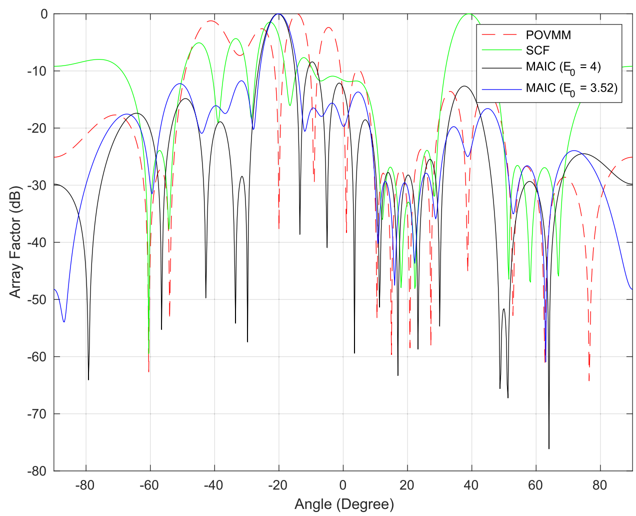

FIGURE 7. Plot of the beampattern of three interference sectors at $\Xi_1 = [-61°, -59°]$, $\Xi_2 = [10°, 30°]$ and $\Xi_3 = [50°, 70°]$. MAIC method performance for $E_0 = 4$ (black line) and $E_0 = 3.52$ (Blue line).

we assume two interference sectors: $\Xi_1 = [-61°, -59°]$ and $\Xi_2 = [50°, 70°]$. MAIC method has been plotted with an energy level of $E_0 = 3.2$. As shown in Fig. 8, the MAIC method managed to steer the mainlobe while keeping a very low interference energy at around -49 dB.

For an energy levels of $E_0 = 3.76$ or above (relativity high mainlobe energy), the MAIC algorithm will have a lower performance as shown in Fig. 9. Although it manages to steer the mainlobe correctly, it was unable to reduce the interference energy below -23 dB due to the very tight mainlobe constraint. The feasible region of the optimization problem is small and, hence, the optimum value prioritizes the mainlobe steering instead of reducing the interference energy.

E. SIDELOBE REDUCTION

In Fig. 10 we examine the proposed algorithm for sidelobe reduction. A couple of sidelobe reduction sectors have been added around the mainlobe and two interference sectors. Namely, we assume four undesired sectors: for the sidelobe

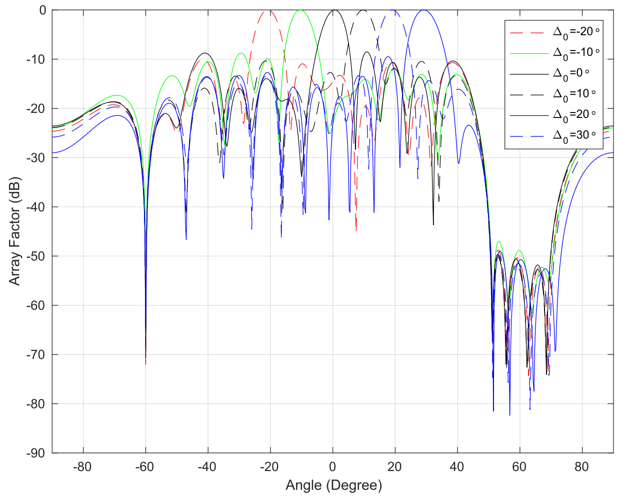

FIGURE 8. Plot of the beampattern of different desired mainlobe directions at $E_0 = 3.2$.

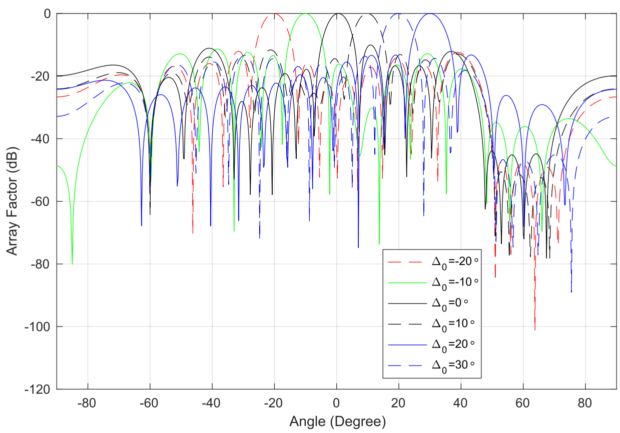

FIGURE 9. Plot of the beampattern of different desired mainlobe directions at $E_0 = 3.76$.

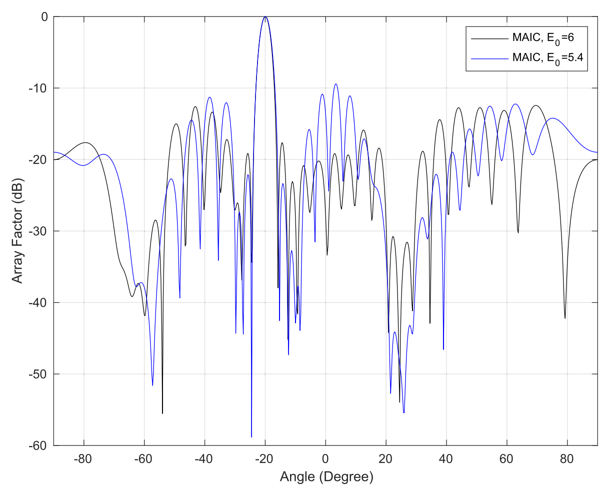

FIGURE 10. Plot of the beampattern of different with four undesired sectors to reduce interference and sidelobe for $E_0 = 6$ and $E_0 = 5.4$.

reduction $\Xi_1 = [-15°, -8°]$, $\Xi_2 = [-30°, -24°]$ and for the interference $\Xi_3 = [20°, 30°]$, $\Xi_4 = [-65°, -55°]$. Note that, the total amount of energy in all directions is a fixed amount, as shown in equation (7). Therefore, if the amount of energy was reduced at the interference sectors, there must be an excess of energy at the other sectors. Nevertheless, it is possible to reduce side lobs by adding more sectors around the main lobe, as shown in the next section.

V. CONCLUSION

Our research accomplishes comprehensive beampattern design for MIMO radar while accommodating constant modulus and mainlobe gain constraints. The core concept of our analytical contribution involves progressively achieving constant modulus (upon convergence) by solving a quadratic program with linear equality and inequality constraints at each step of the sequence. With each problem in the sequence admitting a closed form solution, our method becomes computationally appealing. We establish novel analytical properties of the MAIC algorithm, including a non-decreasing cost function in each iteration and assured convergence. Furthermore, through experimentation, we demonstrate that the proposed MAIC outperforms numerous state-of-the-art methods in terms of beampattern accuracy, even when addressing a gain constrained problem. Future endeavors could explore a wideband beampattern design and delve into further optimality properties of the MAIC solution and the utilization of other array types such as planner arrays.

A. PROOF OF LEMMA 1

Proof: We have the following:

$$\mathbf{x}^H\mathbf{M}\mathbf{x} \geq \lambda_i \mathbf{x}\mathbf{v}_i\mathbf{v}_i^H\mathbf{x} = \lambda_i|\mathbf{v}_i^H\mathbf{x}|^2 \tag{24}$$

this implies,

$$\sqrt{\mathbf{x}^H\mathbf{M}\mathbf{x}} \geq \sqrt{\lambda_i}|\mathbf{v}_i^H\mathbf{x}| \geq \sqrt{\lambda_i}\Re\mathfrak{e}\{\mathbf{v}_i^H\mathbf{x}\} \tag{25}$$

since $\mathbf{x}^H\mathbf{M}\mathbf{x} \geq E_0$ is equivalent to $\sqrt{\mathbf{x}^H\mathbf{M}\mathbf{x}} \geq \sqrt{E_0}$, therefore, $\Re\mathfrak{e}\{\mathbf{v}_i^H\mathbf{x}\} \geq \sqrt{\frac{E_0}{\lambda_i}}$ implies $\mathbf{x}^H\mathbf{M}\mathbf{x} \geq E_0$. □

B. PROOF OF LEMMA 1

Proof: Let $\mathbf{s}^{(n-1)}$ be the optimal solution of $CP^{(n-1)}$. It has been shown in [40] that the new CMC set is feasible i.e. the new constraint include the old solution or $\mathbf{B}_c^{(n)}\mathbf{s}^{(n-1)} = 1$

Here, we need to show that $\mathbf{u}^{(n)T}\mathbf{s}^{(n-1)} \geq \sqrt{\frac{E_0}{\lambda_1}}$, let us define $\bar{\mathbf{u}}$ to be the complex version of $\mathbf{u}$, i.e., $\bar{\mathbf{u}} = \mathbf{v}_1^* e^{-j\arg(\mathbf{v}_1^H\mathbf{x}^{(n-1)})}$ as in (16). Then we have

$$\begin{aligned}
\sqrt{\frac{E_0}{\lambda_1}} &\leq \mathbf{u}^{(n-1)T}\mathbf{s}^{(n-1)} && (26)\\
&= \Re\mathfrak{e}\{\bar{\mathbf{u}}^{(n-1)H}\mathbf{x}^{(n-1)}\} && (27)\\
&= \Re\mathfrak{e}\{\mathbf{v}_1^H\mathbf{x}^{(n-1)}e^{-j\arg(\mathbf{v}_1^H\mathbf{x}^{(n-2)})}\} && (28)\\
&\leq |\mathbf{v}_1^H\mathbf{x}^{(n-1)}e^{-j\arg(\mathbf{v}_1^H\mathbf{x}^{(n-2)})}| && (29)\\
&= \mathbf{v}_1^H\mathbf{x}^{(n-1)}e^{-j\arg(\mathbf{v}_1^H\mathbf{x}^{(n-1)})} && (30)\\
&= \mathbf{u}^{(n)T}\mathbf{s}^{(n-1)} && (31)
\end{aligned}$$

□

C. PROOF OF THEOREM 1

Proof: Denote the feasible sets of $CP^{(n-1)}$ and $CP^{(n)}$ by $\mathcal{F}_{n-1}$ and $\mathcal{F}_n$, respectively. From Lemma 2, $\mathbf{s}^{(n-1)} \in \mathcal{F}_n$. Since $CP^{(n)}$ is a convex problem and $\mathbf{s}^{(n)}$ is the optimal solution of $CP^{(n)}$,

$$\mathbf{s}^{(n-1)T}(\mathbf{R}+\lambda\mathbf{I})\mathbf{s}^{(n-1)} \geq \mathbf{s}^{(n)T}(\mathbf{R}+\lambda\mathbf{I})\mathbf{s}^{(n)} \tag{32}$$

Therefore, the sequence $\{g(\mathbf{s}^{(n)})\}_{n=0}^{\infty}$ is non-increasing. Since $g(\mathbf{s}) \geq 0$ for all values of $\mathbf{s}$, it is bounded below. Hence, it converges to a finite value $s^\star$ according to the monotone convergence theorem [57]. □

REFERENCES

[1] A. Elsayem, H. Elghamrawy, A. Massoud, and A. Noureldin, "Airborne safety in the age of 5G: Assessing the potential interference between C-band and aeronautical radar altimeter," *Int. Arch. Photogramm., Remote Sens. Spatial Inf. Sci.*, vol. 48, pp. 889–894, Jan. 2023.
[2] M. Solkin, "Electromagnetic interference hazards in flight and the 5G mobile phone: Review of critical issues in aviation security," *Transp. Res. Proc.*, vol. 59, pp. 310–318, Jan. 2021.
[3] Air Line Pilots Association. (2023). *Aircraft Operations and Radar Altimeter Interference From 5G*. [Online]. Available: https://www.alpa.org/resources/aircraft-operations-radar-altimeter-interference-5G
[4] A. Aubry, A. De Maio, M. Piezzo, and A. Farina, "Radar waveform design in a spectrally crowded environment via nonconvex quadratic optimization," *IEEE Trans. Aerosp. Electron. Syst.*, vol. 50, no. 2, pp. 1138–1152, Apr. 2014.
[5] A. Aubry, A. De Maio, M. Piezzo, M. M. Naghsh, M. Soltanalian, and P. Stoica, "Cognitive radar waveform design for spectral coexistence in signal-dependent interference," in *Proc. IEEE Radar Conf.*, May 2014, pp. 474–478.
[6] K. D. Shepherd and R. A. Romero, "Radar waveform design in active communications channel," in *Proc. Asilomar Conf. Signals, Syst. Comput.*, Nov. 2013, pp. 1515–1519.
[7] T. Guo and R. Qiu, "OFDM waveform design compromising spectral nulling, side-lobe suppression and range resolution," in *Proc. IEEE Radar Conf.*, May 2014, pp. 1424–1429.
[8] F. Xin, J. Wang, B. Wang, and X. Song, "Waveform design for cognitive radar based on information theory," in *Proc. Int. Conf. Multisensor Fusion Inf. Integr. Intell. Syst. (MFI)*, Sep. 2014, pp. 1–8.
[9] W. Huleihel, J. Tabrikian, and R. Shavit, "Optimal adaptive waveform design for cognitive MIMO radar," *IEEE Trans. Signal Process.*, vol. 61, no. 20, pp. 5075–5089, Oct. 2013.
[10] B. Tang, J. Tang, and Y. Peng, "MIMO radar waveform design in colored noise based on information theory," *IEEE Trans. Signal Process.*, vol. 58, no. 9, pp. 4684–4697, Sep. 2010.
[11] S. Amuru, R. M. Buehrer, R. Tandon, and S. Sodagari, "MIMO radar waveform design to support spectrum sharing," in *Proc. IEEE Mil. Commun. Conf.*, Nov. 2013, pp. 1535–1540.
[12] A. Aubry, A. De Maio, Y. Huang, M. Piezzo, and A. Farina, "A new radar waveform design algorithm with improved feasibility for spectral coexistence," *IEEE Trans. Aerosp. Electron. Syst.*, vol. 51, no. 2, pp. 1029–1038, Apr. 2015.
[13] J. R. Guerci, R. M. Guerci, A. Lackpour, and D. Moskowitz, "Joint design and operation of shared spectrum access for radar and communications," in *Proc. IEEE Radar Conf. (RadarCon)*, May 2015, pp. 0761–0766.
[14] A. Lackpour, A. Rosenwinkel, J. R. Guerci, A. Mody, and D. Ryan, "Design and analysis of an information exchange-based radar/communications spectrum sharing system (RCS3)," in *Proc. IEEE Radar Conf. (RadarConf)*, May 2016, pp. 1–6.
[15] E. Faghand, E. Mehrshahi, and S. A. Ghorashi, "Complexity reduction in beamforming of uniform array antennas for MIMO radars," *IEEE Trans. Radar Syst.*, vol. 1, pp. 413–422, 2023.

[16] M. Skolnik, *Radar Handbook*. New York, NY, USA: McGraw-Hill, 1990.

[17] F. Gini, A. D. Maio, and L. Patton, *Waveform Design and Diversity for Advanced Radar Systems*. London, U.K.: The Institution of Engineering and Technology, 2012.

[18] W. Rowe, P. Stoica, and J. Li, ''Spectrally constrained waveform design,'' *IEEE Signal Process. Mag.*, vol. 31, no. 3, pp. 157–162, May 2014.

[19] L. Guo, H. Deng, B. Himed, T. Ma, and Z. Geng, ''Waveform optimization for transmit beamforming with MIMO radar antenna arrays,'' *IEEE Trans. Antennas Propag.*, vol. 63, no. 2, pp. 543–552, Feb. 2015.

[20] Y.-C. Wang, X. Wang, H. Liu, and Z.-Q. Luo, ''On the design of constant modulus probing signals for MIMO radar,'' *IEEE Trans. Signal Process.*, vol. 60, no. 8, pp. 4432–4438, Aug. 2012.

[21] H. Zang, H. Liu, S. Zhou, and X. Wang, ''MIMO radar waveform design involving receiving beamforming,'' in *Proc. Int. Radar Conf.*, Oct. 2014, pp. 1–4.

[22] S. Sen, ''Constant-envelope waveform design for optimal target-detection and autocorrelation performances,'' in *Proc. IEEE Int. Conf. Acoust., Speech Signal Process.*, May 2013, pp. 3851–3855.

[23] S. Ahmed and M.-S. Alouini, ''MIMO radar transmit beampattern design without synthesising the covariance matrix,'' *IEEE Trans. Signal Process.*, vol. 62, no. 9, pp. 2278–2289, May 2014.

[24] X. Zhang, Z. He, L. Rayman-Bacchus, and J. Yan, ''MIMO radar transmit beampattern matching design,'' *IEEE Trans. Signal Process.*, vol. 63, no. 8, pp. 2049–2056, Apr. 2015.

[25] C. Pan, J. Benesty, and J. Chen, ''Design of directivity patterns with a unique null of maximum multiplicity,'' *IEEE/ACM Trans. Audio, Speech, Language Process.*, vol. 24, no. 2, pp. 226–235, Feb. 2016.

[26] Z. Chen, H. Li, G. Cui, and M. Rangaswamy, ''Adaptive transmit and receive beamforming for interference mitigation,'' *IEEE Signal Process. Lett.*, vol. 21, no. 2, pp. 235–239, Feb. 2014.

[27] P. Stoica, J. Li, X. Zhu, and J. R. Guerci, ''On using a priori knowledge in space-time adaptive processing,'' *IEEE Trans. Signal Process.*, vol. 56, no. 6, pp. 2598–2602, Jun. 2008.

[28] G. Hua and S. S. Abeysekera, ''MIMO radar transmit beampattern design with ripple and transition band control,'' *IEEE Trans. Signal Process.*, vol. 61, no. 11, pp. 2963–2974, Jun. 2013.

[29] Y. Xu, X. Zhao, and Y.-C. Liang, ''Robust power control and beamforming in cognitive radio networks: A survey,'' *IEEE Commun. Surveys Tuts.*, vol. 17, no. 4, pp. 1834–1857, 4th Quart., 2015.

[30] H. He, P. Stoica, and J. Li, ''Wideband MIMO systems: Signal design for transmit beampattern synthesis,'' *IEEE Trans. Signal Process.*, vol. 59, no. 2, pp. 618–628, Feb. 2011.

[31] O. Aldayel, V. Monga, and M. Rangaswamy, ''Tractable transmit MIMO beampattern design under a constant modulus constraint,'' *IEEE Trans. Signal Process.*, vol. 65, no. 10, pp. 2588–2599, May 2017.

[32] W. Roberts, J. Li, P. Stoica, and X. Zhu, ''MIMO radar receiver design,'' in *Proc. IEEE Radar Conf.*, May 2008, pp. 1–6.

[33] H. Deng and B. Himed, ''Interference mitigation processing for spectrum-sharing between radar and wireless communications systems,'' *IEEE Trans. Aerosp. Electron. Syst.*, vol. 49, no. 3, pp. 1911–1919, Jul. 2013.

[34] D. R. Fuhrmann and G. San Antonio, ''Transmit beamforming for MIMO radar systems using signal cross-correlation,'' *IEEE Trans. Aerosp. Electron. Syst.*, vol. 44, no. 1, pp. 171–186, Jan. 2008.

[35] P. Stoica, J. Li, and X. Zhu, ''Waveform synthesis for diversity-based transmit beampattern design,'' *IEEE Trans. Signal Process.*, vol. 56, no. 6, pp. 2593–2598, Jun. 2008.

[36] S. Ahmed, J. S. Thompson, Y. R. Petillot, and B. Mulgrew, ''Unconstrained synthesis of covariance matrix for MIMO radar transmit beampattern,'' *IEEE Trans. Signal Process.*, vol. 59, no. 8, pp. 3837–3849, Aug. 2011.

[37] A. Aubry, A. De Maio, and Y. Huang, ''MIMO radar beampattern design via PSL/ISL optimization,'' *IEEE Trans. Signal Process.*, vol. 64, no. 15, pp. 3955–3967, Aug. 2016.

[38] J. R. Guerci, *Space-Time Adpative Processing for Radar*. Norwood, MA, USA: Artech House, Jul. 2003.

[39] O. Aldayel, V. Monga, and M. Rangaswamy, ''Transmit MIMO beampattern design under constant modulus and spectral interference constraints,'' in *Proc. IEEE Radar Conf. (RadarConf)*, May 2017, pp. 1131–1136.

[40] B. Kang, O. Aldayel, V. Monga, and M. Rangaswamy, ''Spatio-spectral radar beampattern design for coexistence with wireless communication systems,'' *IEEE Trans. Aerosp. Electron. Syst.*, vol. 55, no. 2, pp. 644–657, Apr. 2019.

[41] L. K. Patton and B. D. Rigling, ''Modulus constraints in adaptive radar waveform design,'' in *Proc. IEEE Radar Conf.*, May 2008, pp. 1–6.

[42] L. K. Patton, ''On the satisfaction of modulus and ambiguity function constraints in radar waveform optimization for detection,'' Ph.D. dissertation, Dept. Elect. Eng., Wright State Univ., Dayton, OH, USA, 2009.

[43] B. Friedlander, ''Waveform design for MIMO radars,'' *IEEE Trans. Aerosp. Electron. Syst.*, vol. 43, no. 3, pp. 1227–1238, Jul. 2007.

[44] Z. Wang, Y. Ge, J. Pu, X. Chen, G. Li, Y. Wang, K. Liu, H. Zhang, and Z. Chen, ''1 bit electronically reconfigurable folded reflectarray antenna based on p-i-n diodes for wide-angle beam-scanning applications,'' *IEEE Trans. Antennas Propag.*, vol. 68, no. 9, pp. 6806–6810, Sep. 2020.

[45] G. Cui, H. Li, and M. Rangaswamy, ''MIMO radar waveform design with constant modulus and similarity constraints,'' *IEEE Trans. Signal Process.*, vol. 62, no. 2, pp. 343–353, Jan. 2014.

[46] Z.-Q. Luo, W.-K. Ma, A. M. So, Y. Ye, and S. Zhang, ''Semidefinite relaxation of quadratic optimization problems,'' *IEEE Signal Process. Mag.*, vol. 27, no. 3, pp. 20–34, May 2010.

[47] P. Stoica, H. He, and J. Li, ''On designing sequences with impulse-like periodic correlation,'' *IEEE Signal Process. Lett.*, vol. 16, no. 8, pp. 703–706, Aug. 2009.

[48] Z. D. Zaharis, K. A. Gotsis, and J. N. Sahalos, ''Adaptive beamforming with low side lobe level using neural networks trained by mutated Boolean PSO,'' *Prog. Electromagn. Res.*, vol. 127, pp. 139–154, 2012.

[49] Z. D. Zaharis, I. P. Gravas, P. I. Lazaridis, T. V. Yioultsis, and T. D. Xenos, ''Improved beamforming in 3D space applied to realistic planar antenna arrays by using the embedded element patterns,'' *IEEE Trans. Veh. Technol.*, vol. 71, no. 6, pp. 6145–6157, Jun. 2022.

[50] I. P. Gravas, Z. D. Zaharis, T. V. Yioultsis, P. I. Lazaridis, and T. D. Xenos, ''Adaptive beamforming with sidelobe suppression by placing extra radiation pattern nulls,'' *IEEE Trans. Antennas Propag.*, vol. 67, no. 6, pp. 3853–3862, Jun. 2019.

[51] I. Mallioras, Z. D. Zaharis, P. I. Lazaridis, and S. Pantelopoulos, ''A novel realistic approach of adaptive beamforming based on deep neural networks,'' *IEEE Trans. Antennas Propag.*, vol. 70, no. 10, pp. 8833–8848, Oct. 2022.

[52] I. Mallioras, T. V. Yioultsis, N. V. Kantartzis, P. I. Lazaridis, and Z. D. Zaharis, ''Enhancing adaptive beamforming in 3-D space through self-improving neural network techniques,'' *IEEE Open J. Commun. Soc.*, vol. 5, pp. 1340–1357, 2024.

[53] O. Aldayel, ''Tractable radar waveform design under practical constraints,'' Ph.D. dissertation, Pennsylvania State Univ., University Park, PA, USA, 2017.

[54] K. Alhujaili, X. Yu, G. Cui, and V. Monga, ''Spectrally compatible MIMO radar beampattern design under constant modulus constraints,'' *IEEE Trans. Aerosp. Electron. Syst.*, vol. 56, no. 6, pp. 4749–4766, Dec. 2020.

[55] K. Metwaly, J. Kweon, K. Alhujaili, M. Greco, F. Gini, and V. Monga, ''Interpretable, unrolled deep radar beampattern design,'' in *Proc. IEEE Int. Conf. Acoust., Speech Signal Process. (ICASSP)*, Jun. 2023, pp. 1–5.

[56] V. V. Williams, ''Multiplying matrices faster than coppersmith-winograd,'' in *Proc. 44th Annu. ACM Symp. Theory Comput.*, May 2012, pp. 887–898.

[57] H. L. Royden and P. Fitzpatrick, *Real Analysis*, 4th ed. Upper Saddle River, NJ, USA: Prentice-Hall, 2010.

OMAR ALDAYEL (Member, IEEE) received the B.S. degree from King Saud University, Riyadh, Saudi Arabia, in 2007, the M.S. degree from the KTH—Royal Institute of Technology, Stockholm, Sweden, in 2011, and the Ph.D. degree in electrical engineering from The Pennsylvania State University, University Park, PA, USA, in 2017. He was with King Saud University as a Lecturer, from 2011 to 2013, where he is currently an Assistant Professor with the Department of Electrical Engineering. His research interests include statistical signal processing and optimization theory with its application to radar signal processing and wireless communications.